IEEE Access
Multidisciplinary | Rapid Review | Open Access Journal

Received December 10, 2017, accepted January 15, 2018, date of publication January 23, 2018, date of current version March 15, 2018.

Digital Object Identifier 10.1109/ACCESS.2018.2795538

Wavelet-Based Beamforming for High-Speed Rotating Acoustic Source

WANGQIAO CHEN[1] AND XUN HUANG[1,2], (Member, IEEE)

[1]State Key Laboratory of Turbulence and Complex System, Department of Aeronautics and Astronautics, College of Engineering, Peking University, Beijing 100871, China

[2]Department of Mechanical and Aerospace Engineering, The Hong Kong University of Science and Technology, Hong Kong

Corresponding author: Xun Huang (huangxun@pku.edu.cn)

This work was supported in part by the National Science Foundation of China under Grant 11561130148, in part by the Ministry of Industry and Information Technology of China under Grant MJ-2015- F-012-03, and in part by the Research Grants Council of the Hong Kong Special Administrative Region under Grant 16205317.

ABSTRACT In this paper, a novel wavelet-based beamforming approach is proposed for sensor arrays to produce acoustic images of high-speed rotating sources. First, the associated Green's function is developed based on the Morse wavelet which also accounts for the Doppler effect. Then, the beamforming operation can be conducted simply as an inversion in the time–frequency domain. Compared with the conventional Fourier-transform-based beamforming method, the proposed wavelet-based approach shows significant improvement in the real-time imaging quality and background noise suppression, which is illustrated by representative numerical simulations and experimental demonstrations. The proposed wavelet-based beamforming approach is particularly useful for the acoustic imaging in the time–frequency domain for moving sources of a high-subsonic speed and will find applications, such as audio guidance and low-noise airplane design, in robotics and aerospace industry.

INDEX TERMS Beamforming, wavelet, sensor array, acoustic imaging.

I. INTRODUCTION

Beamforming [1] enables a microphone array to track and to produce acoustic images of sources of interest [2]–[4]. Various applications can be found in radar, sonar, communications and medical imaging [5]–[7], where adaptive beamforming [8], [9] has been mostly adopted mainly due to its high spatial resolution. However, this method is susceptible to background noise and interference [10], [11]. The main focus of this work is typical rotor noise generated by quadcopter type unmanned aerial vehicle (UAV) systems, where the noise tests are often plagued by severe background noise and interference either from testing facilities [11] or from rotor-to-rotor interactions [12]. Currently, for many aerospace and underwater noise measurement applications [13]–[15], conventional delay-and-sum type Fourier-transform-based beamforming methods [14], [16] remain popular for flow-induced acoustic problems due to their robustness, which suppresses the (usually) uncorrelated background noise and interference by averaging samples in frequency domain. To further improve the real-time imaging and background noise suppression performance, we examined the deconvolution type postprocessing approach [11] and had previously proposed a so-called observer method [17] and a compressive sensing based method [18]. However, care should be taken in the usage of these methods as block averaging of Fourier transform results in the frequency domain would smear the resultant acoustic images across the moving trajectories and thus should only be effective for relatively low-speed (or stationary) noise targets (e.g. wind turbines [19]). Nevertheless, the inherent physics, namely the Doppler effect, should still remain the same as those in [19] as long as the moving speed is subsonic. For high-subsonic-speed noise sources such as rotating fans, a number of previous works [20]–[23] have considered rotating microphone rakes, and the imaging performance heavily depends on the exact tracing of instantaneous rotation speeds. Motivated by this physical issue, the current work applies the wavelet transform rather than the Fourier transform in the development of the array beamforming approach, with a particular focus on fan and propeller noise measurement applications.

Recent developments in the wavelet-based beamforming methods based on uniform linear arrays [24], [25] have demonstrated multiresolution and time-frequency

analysis capabilities in geological detection [26] and brain research [27]; the wavelet-based approach is yet to be demonstrated in aircraft propulsion applications. Fan and propeller noise is one of the most dominant noise sources for current aircraft (including UAV) and public concern regarding the adverse psychological and environmental effects of aircraft noise emission has led to stringent regulations faced by the civil aviation industry; accurate acoustic imaging can aid the development and testing of low-noise designs. In fan and propeller acoustic noise tests Doppler effect is observed; the rotation of sound sources relative to an observer results in frequency shifts, which in turn leads to time-variant Green's function. De-dopplerization [19], [23] technique may be adopted to remove frequency shifts by first processing the samples before the conduction of beamforming [19], [23], [28]. Instead of this usual preprocessing, a wavelet transform, which gives the time-frequency representations of the sampled signal, enables us to develop our new beamforming approach based on relatively straightforward analyses.

Previous works on the application of acoustic beamforming methods for rotating sources can be categorized into time domain methods and frequency domain methods: Sijtsma [29] has applied an appropriate time-delay to each samples to reconstruct a stationary imaging plane; Wolfram and Christian [23] have proposed a similar method for a rotating array to reconstruct samples but in the frequency domain. To simply apply a time-delay, all sensors have to form a concentrically circular array, which is difficult and will impose an undesirable effect on the final beamforming resolution. In contrast, Dougherty and Walker [22] have applied a different resampling strategy to manipulate samples in a rotating coordinate frame. In addition, a beamformer for moving sources has been developed in the frequency domain by reconstructing the associated point spread function [30]. Michael [31] and Carley [32], [33] has studied the sound field of rotating monopole and propeller, and developed the associated radiation field in either spherical or cylindrical coordinates.

Different from the above methods, the wavelet-based beamforming method proposed in this work directly incorporates the wavelet transform and the Doppler effect into the Green's function, which produces acoustic images in the time-frequency domain. In short, the proposed method is a combination of the frequency-domain and time-domain beamforming methods and the related developments for rotating sources, to the best of our knowledge, have never been reported previously, which constitutes the main contribution of this work. To facilitate potential users, the algorithm for the proposed method is summarized and included in this paper. After some slight modifications, the proposed method should be applicable to sound sources of arbitrary high-speed motions as well. The remaining part of this paper is organized as follows. Section II gives the theoretical background of the proposed wavelet-based method with a more detailed development included in the appendix. Then, Sec. III gives the numerical and experimental studies and compared the imaging performance of the proposed wavelet-based beamforming method to the performance of the classical Fourier-transform-based beamforming method. Finally, Sec. IV concludes the present research.

II. WAVELET-BASED BEAMFORMING

To facilitate readers, we propose the main mathematical equations of the new wavelet-based beamforming method below along with the essential concepts behind the equations and the corresponding explanations. A more detailed theoretical development is given in the appendix. First, the array beamforming for high-speed moving sources of imaging frequency ω_i in the position $\vec{x}_b$ at an imaging time t_i (from the source perspective) can be written as

$$\mathfrak{b}(\vec{x}_b, \omega, t_i) = \vec{w}^*(\vec{x}_b, t_i) A(\vec{x}_b, \omega_i, t_i) \vec{w}(\vec{x}_b, t_i), \tag{1}$$

where $(\cdot)^*$ denotes the complex conjugate, A is the cross spectral matrix, and the vector $\vec{w}(\vec{x}_b, t_i)$ is array weight. Theoretically, Eq. (1) acts as a spatial filter that rejects background noise and interference from other sources. The weight vector is calculated from the so-called array propagation vector and, therefore, takes the following form as

$$\vec{w}(\vec{x}_b, t_i) = \frac{C(\vec{x}_b, t_i)}{||C(\vec{x}_b, t_i)||}, \tag{2}$$

where $||\cdot||$ denotes the L2-norm, that is,

$$||C(\vec{x}_b, t_i)|| = \left(\sum_{n=1}^{N} C_n(\vec{X}_n, \vec{x}_b, t_i)\, C_n^*(\vec{X}_n, \vec{x}_b, t_i) \right)^{\frac{1}{2}}, \tag{3}$$

where $C_n(\vec{X}_n, \vec{x}_b, t_i)$ is the n-th element of the vector $C(\vec{x}_b, t_i)$, $\vec{X}_n$ is the associated location of the n-th sensor, and N is the number of array sensors. To further illustrate the inherent physics, here we simply consider a point type source and the corresponding array propagation vector is

$$C_n(\vec{X}_n, \vec{x}_b, t_i) = \frac{\alpha^2(\vec{X}_n, \vec{x}_b, t_i)\beta(\vec{X}_n, \vec{x}_b, t_i)}{4\pi |\vec{X}_n - \vec{x}_b|}, \tag{4}$$

where $|\vec{X}_n - \vec{x}_b|$ represents the distance between the n-th sensor (at $\vec{X}_n$) of the array and the b-th gridpoint (at $\vec{x}_b$) on the imaging plane, α is caused by the Doppler effect and β is caused by the nearfield amplification effect. A more detailed derivation of α and β can be found in the appendix. Furthermore, the cross spectral matrix, $A(\vec{x}_b, \omega_i, t_i)$, in Eq. (1) is defined as

$$A(\vec{x}_b, \omega_i, t_i) = Y(\vec{x}_b, \omega_i, t_i) Y^*(\vec{x}_b, \omega_i, t_i), \tag{5}$$

where $Y(\vec{x}_b, \omega_i, t_i)$ represents the time-frequency outputs of the array. In classical delay-and-sum beamforming, this output is actually independent of the imaging gridpoint $\vec{x}_b$. Nevertheless, given a rotating source of the frequency ω_i, the n-th sensor will perceive a different imaging frequency ω_i^n owing to the Doppler effect, that is,

$$\omega_i^n = \omega_i \cdot \alpha(\vec{X}_n, \vec{x}_b, t_i). \tag{6}$$

Hence, $Y(\vec{x}_b, \omega_i, t_i)$ becomes to be dependent of $\vec{x}_b$ and $\vec{X}_n$. As a result, it is better to denote the output from the n-th sensor as $Y_n(\vec{X}_n, \vec{x}_b, \omega_i^n, t_i + R_n/c_0)$, where c_0 is the speed of sound and Y_n is the time-frequency result from the n-th sensor at $\vec{X}_n$ by applying continuous wavelet transform.

In this work, we adopt the generalized Morse wavelet for its capability that unifies many wavelet types [34]. The Morse wavelet is usually defined in the frequency domain as

$$\Psi_{\mathcal{P},\gamma}(\omega) = \int_{-\infty}^{\infty} \psi_{\mathcal{P},\gamma}(t) e^{-i\omega t} dt = U(\omega) a_{\mathcal{P},\gamma} \omega^{\frac{\mathcal{P}^2}{\gamma}} e^{-\omega^\gamma}, \tag{7}$$

where $a_{\mathcal{P},\gamma}$ is used to normalize the wavelet, $U(\omega)$ denotes the unit step function, and $\mathcal{P}$ and γ are parameters that control the form of the wavelet. Reference [34] has conducted a parametric study of parameters in terms of the so-called Heisenberg area, and this work adopts the default values used by MATLAB, i.e., $\gamma = 3$ and $\mathcal{P}^2 = 60$, which yield the most symmetric, Gaussian and most nearly time-frequency concentrated wavelets and, therefore, hopefully ensure a satisfactory performance. For brevity, the subscripts $\mathcal{P}$ and γ will be omitted in the rest of this paper when no confusion will arise. Next, we use this bandpass type continuous wavelet transform [34] to study the time- and frequency-localized variability of the sound pressure field, and obtain P_n as

$$\begin{aligned} &P_n(\vec{X}_n, \vec{x}_b, s, t) \\ &\quad = \lim_{\Delta t \to 0} P_n(\vec{X}_n, \vec{x}_b, s, t + \Delta t) \\ &\quad = \lim_{\Delta t \to 0} \frac{1}{s} \int_{-\infty}^{\infty} p(\vec{X}_n, \vec{x}_b, t + \tau') \psi^*\left(\frac{\Delta t - \tau'}{s}\right) d\tau', \end{aligned} \tag{8}$$

where $p(\vec{X}_n, \vec{x}_b, t + \tau')$ denotes the sensor samples at time $t + \tau'$, where t is usually equal to $t_i + R_n/c_0$, ψ is defined in Eq. (7), and $P_n(\vec{X}_n, \vec{x}_b, s, t)$ is the corresponding continuous wavelet transform result of the n-th sensor at time t. From Eq. (8), we can further have

$$\begin{aligned} P_n(\vec{X}_n, \vec{x}_b, s, t) = i\omega_i C_n(\vec{X}_n, \vec{x}_b, t_i) e^{i\omega_i t_i} \cdot q_0 \\ \cdot \lim_{\Delta t \to 0} \frac{1}{s} \int_{-\infty}^{\infty} e^{i\omega_i^n \tau'} \psi^*\left(\frac{\Delta t - \tau'}{s}\right) d\tau', \end{aligned} \tag{9}$$

The result of Eq. (9) is a function of time t and the scale parameter s (of wavelets). The latter is related to the angular frequency ω as follows,

$$\omega(s) = 2\pi \frac{f_0}{s} \cdot T_s, \tag{10}$$

where f_0 is the peak frequency and T_s is the sampling time interval. Thus, we can rewrite $P_n(\vec{X}_n, \vec{x}_b, s, t_i + R_n/c_0)$ as $P_n(\vec{X}_n, \vec{x}_b, s(\omega), t_i + R_n/c_0)$. From Eqs. (8) and (9), we can get the wavelet transform output at the frequency ω_i^n and time $t_i + R_n/c_0$,

$$Y_n(\vec{X}_n, \vec{x}_b, \omega_i^n, t_i + R_n/c_0) = P_n(\vec{X}_n, \vec{x}_b, s(\omega_i^n), t_i + R_n/c_0). \tag{11}$$

We wish to emphasize that Eqs. (8)–(9) and (11) assume a single moving point source at varying $\vec{x}_b$, and such a derivation assists the understanding of the relation between the samples and the propagation vector (see Eq. (9)). Nevertheless, a practical sensor will measure sound waves from all possible sources at various different locations simultaneously and the measurement outcome p (see Eq. (8)) should be independent of the source positions. Furthermore, the proposed new beamforming method utilizes the time-frequency analysis capability of the wavelet transform, which enables us to dynamically capture a time- and frequency-varying source. The multiscale and multiresolution analysis, which is the other important capability of the wavelet transform, is not considered in the current manuscript and the related work will be reported in the follow-up paper. On the other hand, if a sound source is stationary, $\alpha(\vec{X}_n, \vec{x}_b, t_i) = \beta(\vec{X}_n, \vec{x}_b, t_i) \equiv 1$, and it will be easy to see that the above wavelet-based beamforming method can be simplified to conventional Fourier-based beamforming.

Figure 1 shows the steps of the proposed wavelet-based beamforming method, which can be categorized into two types of activities, data related activities and parameter related activities. The steps of the algorithm are summarized as follows:

1) Parameter related activities: we calculate time delay (R_n/c_0) for each sensor;
2) Data related activities: given t_i, calculate the continuous wavelet transform for each sensor;
3) Parameter related activities: calculate α and β;
4) Data related activities: calculate ω_i^n and prepare the array outputs Y;
5) Parameter related activities: calculate the weight vector $\vec{w}$, and the cross spectral matrix A;
6) Data related activities: calculate the beamforming outputs. Done.

III. NUMERICAL SIMULATION AND EXPERIMENTAL DEMONSTRATION

We first prepare some numerical cases to verify and validate the proposed new beamforming method. Figure 2 shows the coordinates of an array with 63 sensors that form multiple spiral arms, which is one of the optimal array designs in terms of sidelobe suppression [35] and, therefore, has been adopted in this work. In the simulation, a high-speed rotating point source of 3 kHz is located 1 m away from the array, and the rotating speed is set between 6 k revolutions per minute (RPM) and 9 kRPM (common for industry applications). It is easy to develop an analytic solver that gives the corresponding sound pressure predictions at each array sensor, and the sampling rate is set to 40 kHz for the following numerical simulations. In addition, most industry applications are subject to serious background noise and interference. To reflect this negative effect, we intentionally superimpose a random noise into the above analytical predictions to simulate the required signal-to-noise ratio.

First, we try classical Fourier-transform-based beamforming method. Figure 3 shows the corresponding results based

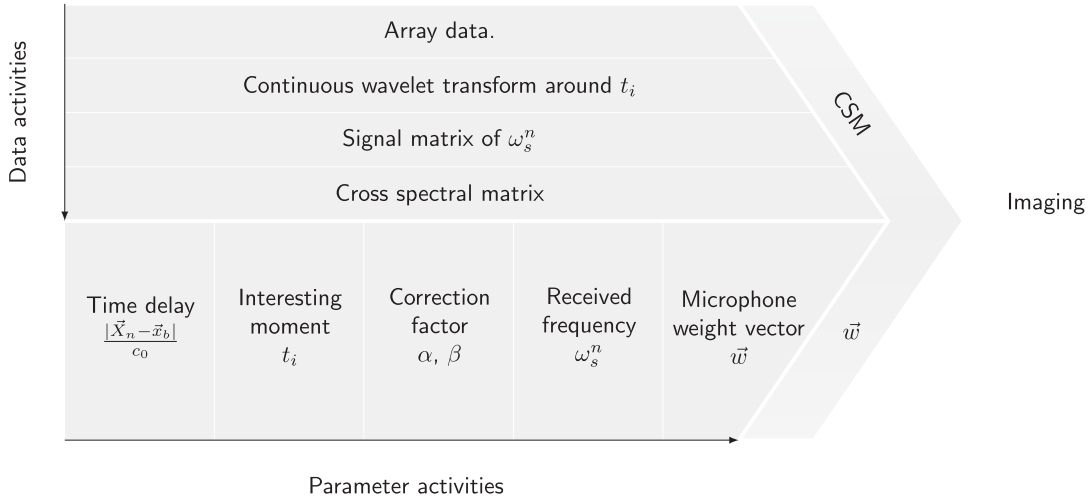

FIGURE 1. Steps of the wavelet-based beamforming in the time-frequency domain. From the top to the central are the activities for the acoustic pressure data. From the left to the right are the activities for the parameters in every step.

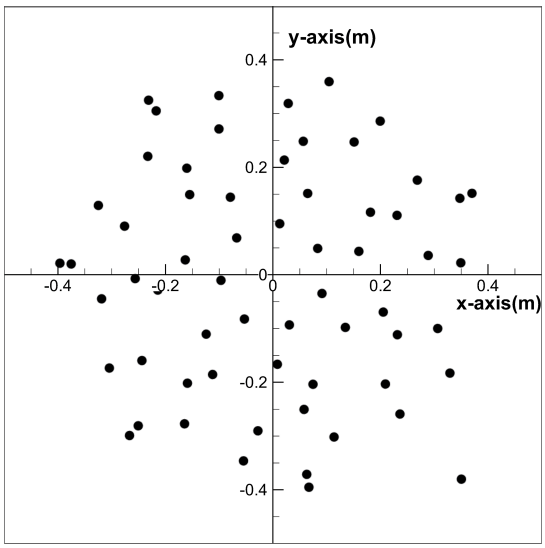

FIGURE 2. The logarithmic spiral layout of the array with 63 sensors used in the numerical simulations.

on one-block of samples with the associated time duration 0.5 ms. The amplitudes of all acoustic images are normalized with respect to the amplitude of the sound source. It can be seen that these short-time Fourier-transform-based beamforming results grossly trace the rotating source, but the poor signal-to-noise ratio (SNR $= -23$ dB for the current case) deteriorates the quality of images substantially. The top panels of Fig. 4 show that an increased time window (from 0.5 ms to 3.3 ms, the corresponding rotating trajectories of the source are highlighted in dashed fan-shapes) slightly suppresses the background noise interference. On the other hand, it is well known that such a compromise, mainly due to incoherent background noise and/or interferences, can be improved by performing statistical averaging of Fourier transform results. For example, the bottom panels of Fig. 4 show the beamforming results based on the averages of many blocks (and the whole duration is 0.5 s). It can be seen that the background noise and interferences are largely suppressed. However, with no surprise, the resultant images of the source will cover the whole rotating trajectories (in 0.5 s). Furthermore, for the set-up with a window of 0.5 ms, the corresponding block-averaging result actually suffers a large loss of the dynamic range (the colorbar dwindles from 12 dB to 4 dB).

The Doppler effect is not considered in the above classical beamforming, which means that no prior knowledge of the rotating source is utilized. Nevertheless, given this knowledge, the wavelet-based beamforming can be conducted specifically for each gridpoint on the imaging plane, which could help to produce better beamforming results. Figure 5 shows the corresponding wavelet-based beamforming results. The set-ups and the simulated array samples are the same as those used in Figs. 3 and 4 and the knowledge of the rotating speed is utilized in the wavelet-based beamforming, i.e., from Eq. (1) to Eq. (11). Compared to Fig. 3, Fig. 5 shows that the proposed wavelet-based beamforming produces instantaneous acoustic images that correctly trace the rotating source as well as substantially reject the background noise, with no sacrifice of dynamic ranges. Figures 3–5 show the results at 6 kRPM and similar conclusion can be drawn from the results at other set-ups with higher RPM (up to 9 kRPM in the current simulations). Overall, the numerical simulations show that the proposed new wavelet-based beamforming approach outperforms the classical beamforming approach in terms of time-frequency analysis capability and imaging quality.

Next, we prepare an investigative experimental demonstration of the proposed wavelet-based beamforming in a small anechoic chamber (2.2 m $\times$ 2.2 m $\times$ 2 m) at Peking University. Figure 6 shows the experimental set-up. The propeller

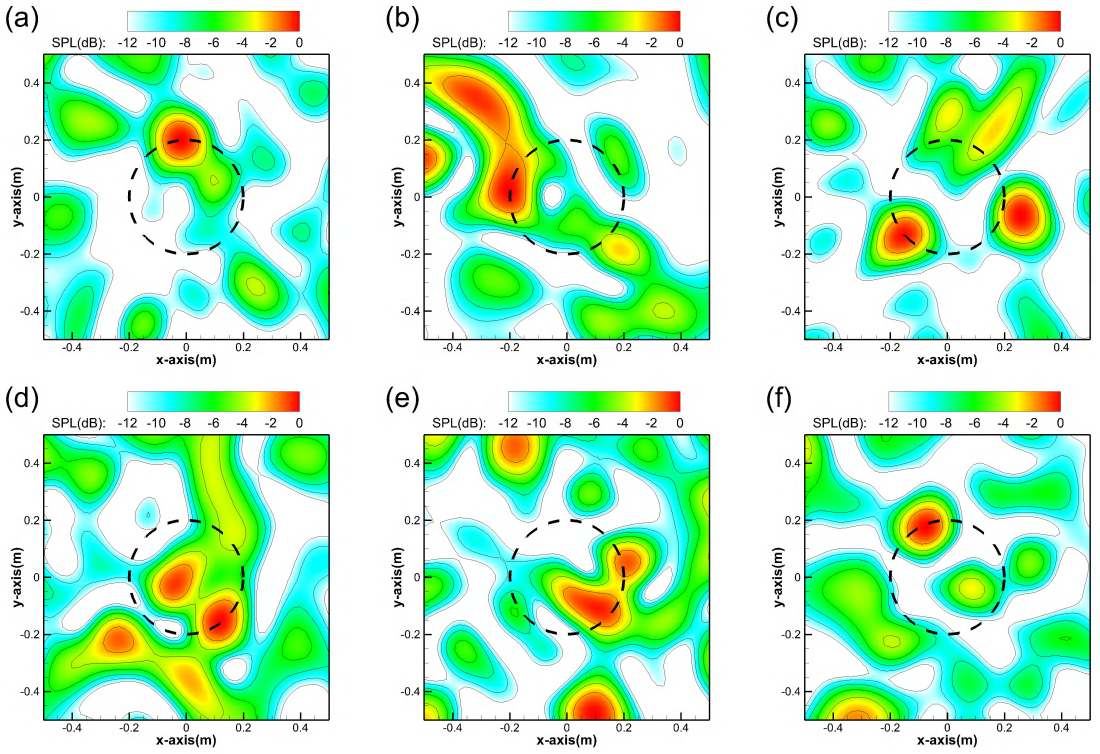

FIGURE 3. The classical beamforming results for a whole rotating period (0 to 2π, from (a) to (f)). The time window chosen for short-time Fourier transform in 0.5 ms. The rotating speed of the source of 3 kHz is 6 kRPM. The signal-to-noise ratio is −23 dB.

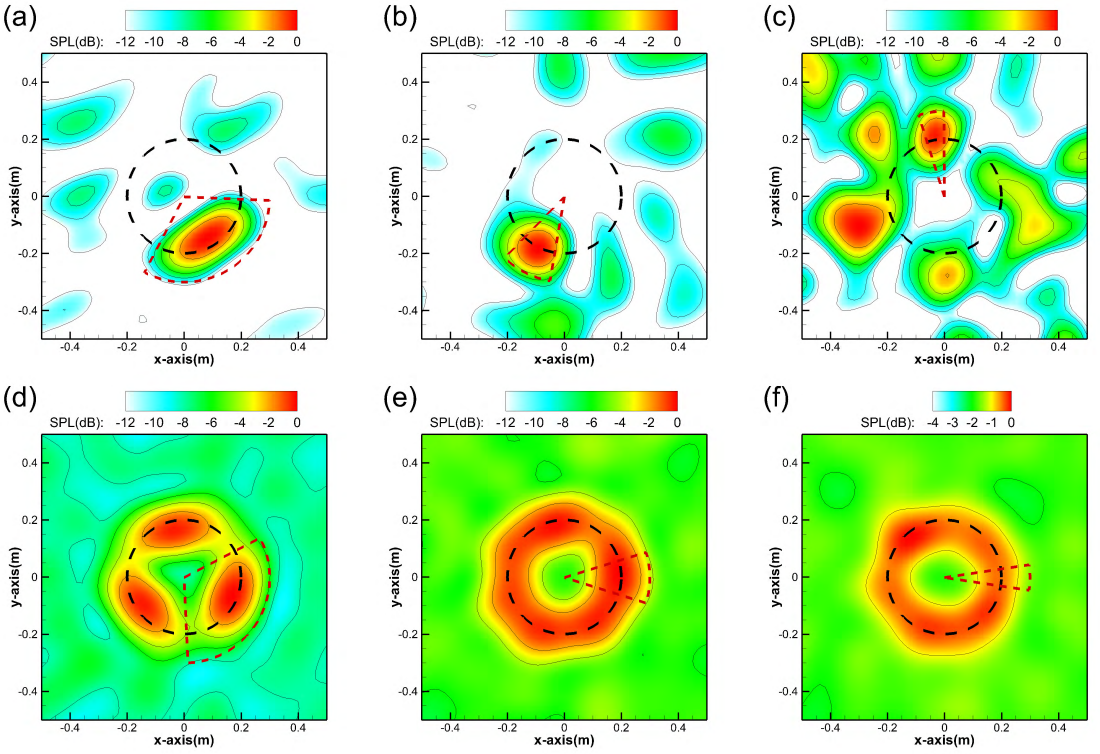

FIGURE 4. The classical beamforming results at a certain rotating angle, where (a)-(c) with one-block of samples and (d)-(f) with many blocks of samples (and the whole duration is 0.5 s), and the window time is (left panels) 3.3 ms, (middle panels) 1 ms and (right panels) 0.5 ms, respectively. Other set-ups are the same as those in Fig. 3.

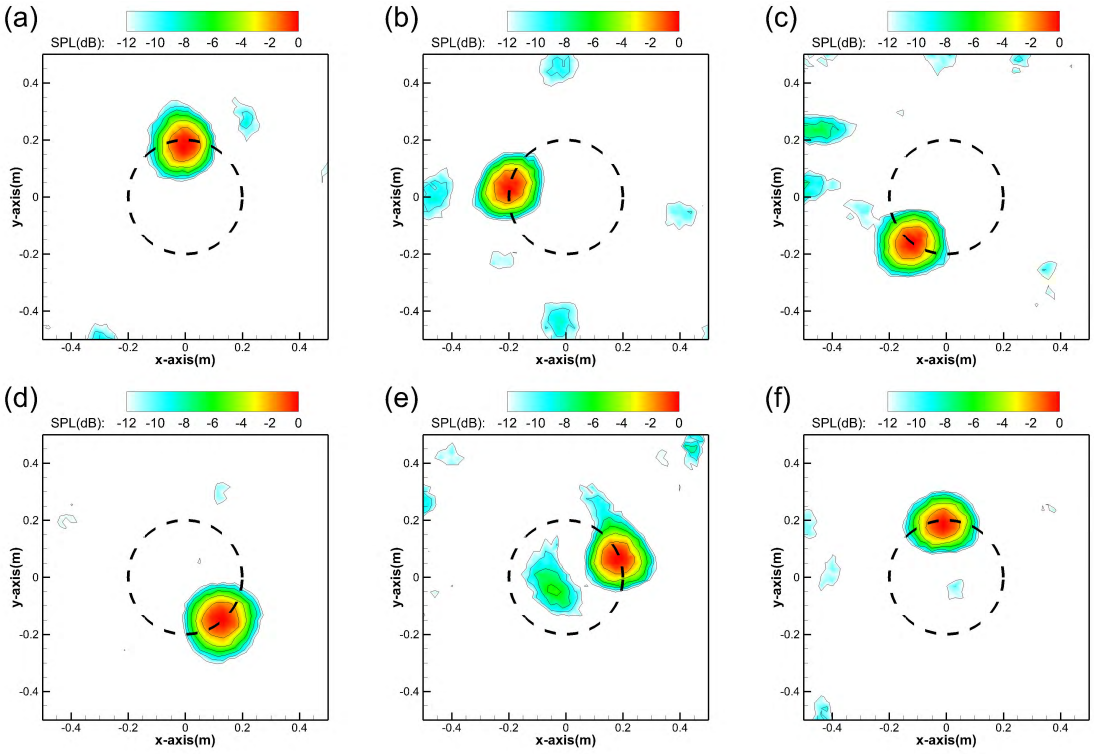

FIGURE 5. The instantaneous wavelet-based beamforming results at various time steps. Other set-ups are the same as those in Fig. 3.

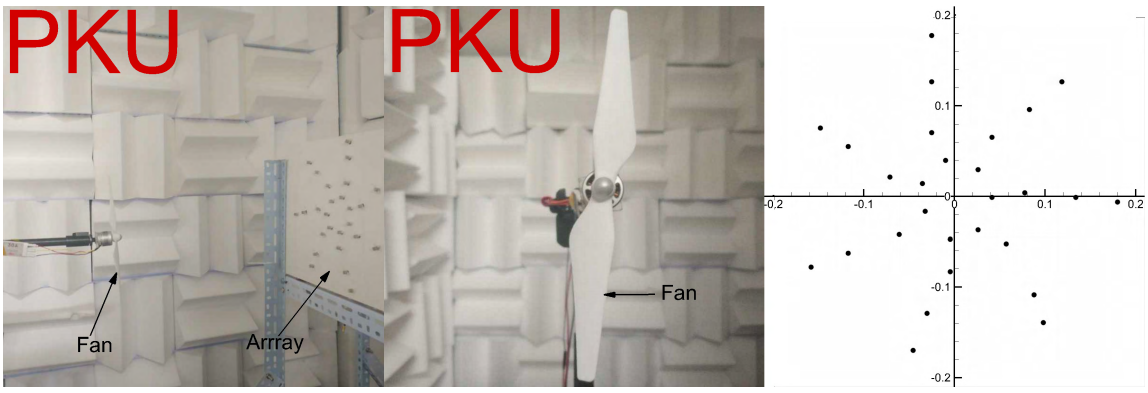

FIGURE 6. The experimental set-up in the anechoic chamber at Peking University, where (left) the whole set-up, (middle) the propeller system, and (right) the layout of the array sensors.

(a 9450 self-tightening type) with the radius of 0.12 m is from an UAV of DJI^{TM}. In this experiment, considering the capability of the driven motor capability, the rotation speed is set to 3 kRPM, and the distance between the microphone array and the rotation propeller is 0.5 m. The array consists of 28 high-precision microphones (BSWA MPA 451) with the sensitivity of -50 ± 5 dBV/Pa. The size of the array is 0.35 m $\times$ 0.35 m and the effective diameter is 0.3 m. An NI PXI-1033 chassis with two 24-bit PXI-4496 cards are used to simultaneously sample the 28-channels of microphones at 40 k samples/s. Physically, the dominant noise source of this rotating propeller is dipole type (mainly caused by pressure force oscillations especially at the rotor tips). Figure 7 shows the corresponding acoustic images from 2 kHz to 5 kHz, by using the proposed new wavelet-based beamforming and classical beamforming approaches, respectively. For the former one, the beamforming results are always instantaneous because the wavelet transform produces time-frequency analysis. For the latter one, however, the beamforming results are produced by adopting the Fourier transform with one block of samples (1 ms duration). Figure 7 shows that the wavelet-based beamforming can identify two dominant noise sources at the two tips of the propeller at most frequency set-ups. In contrast, the classical beamforming usually just

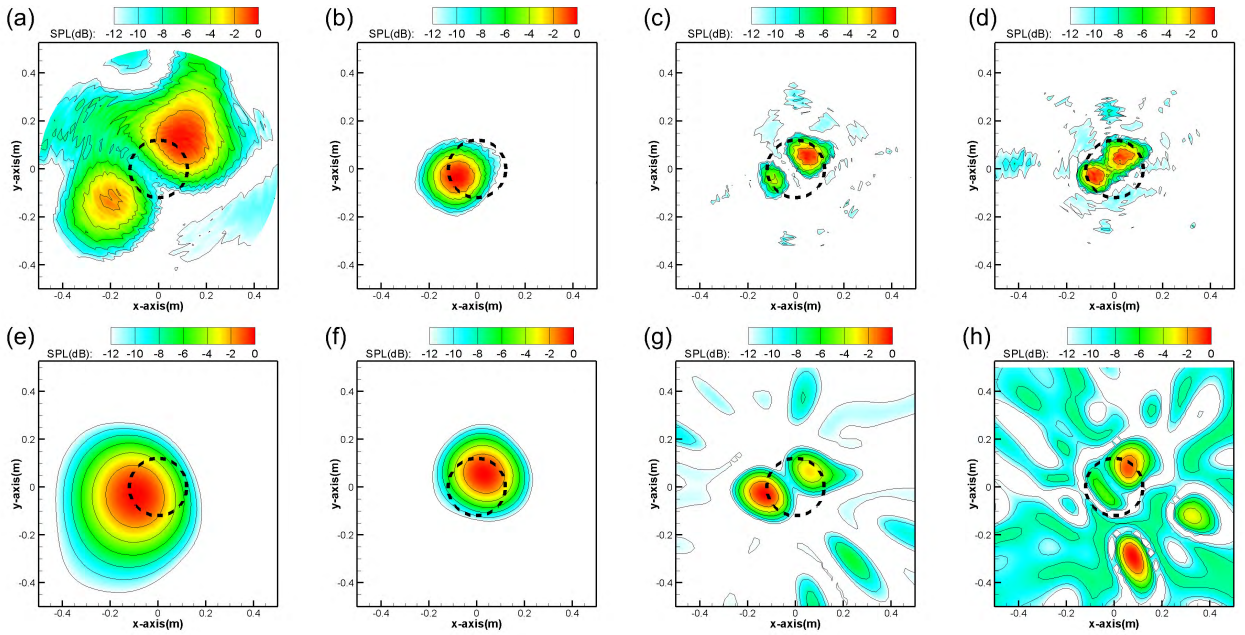

FIGURE 7. The experimental results, where (top) with the wavelet-based beamforming and (bottom) with the classical beamforming. The rotating speed is 3 kRPM, and the beamforming results are at (a)(e) 2 kHz, (b)(f) 3 kHz, (c)(g) 4 kHz, and (d)(h) 5 kHz.

identifies one source during the current tests. Furthermore, the background noise interference is suppressed better by using the wavelet-based beamforming method than does by the classical beamforming method. Overall, these preliminary experimental results successfully demonstrate the capability and benefit of the new wavelet-based beamforming method.

IV. SUMMARY

Here we have developed a new array beamforming method based on the Morse wavelet transform and given the corresponding numerical and experimental investigations, which constitute the essential contribution of this work.

This approach relies on the Doppler effect correction and a high-speed rotating point source model. The whole time-frequency algorithm for acoustic imaging is summarized in Sec. II. Furthermore, we have illustrated the performance of the proposed method by preparing a range of numerical simulations and experimental tests. The most important observations are summarized here. The former classical Fourier-transform-based beamforming method is effective and generic, does not require prior information about the fan noise and guarantee to produce statistically correct inversion results. In contrast, the new wavelet-based beamforming method can incorporate the Doppler effect in a straightforward way, produce acoustic images in the time-frequency domain, and satisfactorily reject background noise and interference. Overall, the concept behind the proposed array beamforming method is very straightforward and should be easy to follow and implement by interested readers. We believe that this work should extend the current array beamforming capability and help the design and evaluation of low-noise propeller systems for robotics and aerospace applications.

APPENDIX

With no loss of generality, we first consider a point source of the form $q(t) = q_0\, e^{i\omega_i t}$ in a uniform and stationary medium, where q is the volume flux and q_0 is the associated amplitude, ω_i is the angular frequency, and the density of the medium is a nondimensionalized unit value. Furthermore, we assume that the source moves from $\vec{x}_0$ at time 0 with a velocity of $\vec{v}(t)$. The associated sound pressure field p can be described by the associated governing equation as follows:

$$\left(\frac{1}{c_0^2}\frac{\partial^2}{\partial t^2} - \nabla^2\right) p = \frac{\partial}{\partial t}\left(q(t)\delta\left(\vec{x} - \int_0^t \vec{v}(\tau)\cdot d\tau - \vec{x}_0\right)\right), \tag{12}$$

where c_0 is the speed of sound, δ is the Dirac delta function, and $\vec{x}$ is the space coordinates. Next, we use the relationship between the velocity potential and acoustic pressure, $p = -\partial\phi/\partial t$. We can rewrite the Eq. (13) as:

$$\left(\frac{1}{c_0^2}\frac{\partial^2}{\partial t^2} - \nabla^2\right) \phi = -q(t)\delta\left(\vec{x} - \int_0^t \vec{v}(\tau)\cdot d\tau - \vec{x}_0\right). \tag{13}$$

The solution for the velocity potential based on the free field Green's function is given by

$$\phi(\vec{x}, t) = \int_{-\infty}^{\infty} \frac{-q(t - \frac{|\vec{x}-\vec{x}'|}{c_0})\delta\left(F(\vec{x}')\right)}{4\pi|\vec{x} - \vec{x}'|} d\vec{x}', \tag{14}$$

where $F(\vec{x}')$ is defined as follows:

$$F(\vec{x}') = \vec{x}' - \int_0^{t-\frac{|\vec{x}-\vec{x}'|}{c_0}} \vec{v}(\tau)\cdot d\tau - \vec{x}_0. \tag{15}$$

Next, we consider $F(\vec{x}') = 0$ when $\vec{x}' = \vec{x}_b$, where $\vec{x}_b$ is the source location at time t_i, satisfying

$$t_i \triangleq t - \frac{|\vec{x}-\vec{x}_b|}{c_0}. \tag{16}$$

Then, we utilize the following Jacobian property of Dirac δ function:

$$\delta\left(F(\vec{x}')\right) = \left|\frac{\partial F(\vec{x}_b)}{\partial \vec{x}'}\right|^{-1} \delta(\vec{x}' - \vec{x}_b). \tag{17}$$

Thus, the solution of velocity potential is

$$\phi(\vec{x}, \vec{x}_b, t) = \frac{-q(t - \frac{|\vec{x}-\vec{x}_b|}{c_0})}{4\pi|\vec{x}-\vec{x}_b|} \cdot \left|\frac{\partial F(\vec{x}_b)}{\partial \vec{x}'}\right|^{-1}. \tag{18}$$

Here we define $\vec{X}_n$ as the associated location of the n-th sensor, and $|\vec{X}_n - \vec{x}_b|$ represents the distance between the n-th sensor (at $\vec{X}_n$) of the array and the source's location $\vec{x}_b$ at an instantaneous time t_i, which is the generation time of the signal, which will be received by the n-th sensor at location $\vec{X}_n$ at time t. We can rewrite Eq. (18) as

$$\phi(\vec{X}_n, \vec{x}_b, t) = \frac{-q(t_i)}{4\pi|\vec{X}_n - \vec{x}_b|} \cdot \alpha(\vec{X}_n, \vec{x}_b, t_i), \tag{19}$$

where $\alpha(\vec{X}_n, \vec{x}_b, t_i)$ is due to the Doppler effect, that is,

$$\begin{aligned}\alpha(\vec{X}_n, \vec{x}_b, t_i) &= \left|\frac{\partial F(\vec{x}_b)}{\partial \vec{x}'}\right|^{-1} = \frac{dt_i}{dt} \\ &= \left(1 + \frac{\vec{v}(t_i)(\vec{x}_b - \vec{X}_n)}{c_0|\vec{X}_n - \vec{x}_b|}\right)^{-1}.\end{aligned} \tag{20}$$

Then, the solution of acoustic pressure is given by

$$p(\vec{X}_n, \vec{x}_b, t) = \frac{\partial}{\partial t}\left(\frac{q(t_i)}{4\pi|\vec{X}_n - \vec{x}_b|} \cdot \alpha(\vec{X}_n, \vec{x}_b, t_i)\right). \tag{21}$$

Given the form of a point source $q(t) = q_0 e^{i\omega t}$, the associated acoustic pressure can be written as

$$\begin{aligned}&p(\vec{X}_n, \vec{x}_b, t) \\ &= \frac{1}{4\pi}\left(\frac{dq(t_i)}{dt_i}\frac{dt_i}{dt}\frac{\alpha}{|\vec{X}_n - \vec{x}_b|} - q(t_i)\frac{\alpha^2}{R_n^2}\frac{d}{dt_i}(\frac{R_n}{\alpha})\frac{dt_i}{dt}\right) \\ &= \frac{i\omega_i q(t_i)\alpha^2}{4\pi|\vec{X}_n - \vec{x}_b|}\left(1 + i\frac{\alpha}{\omega_i|\vec{X}_n - \vec{x}_b|}\frac{d}{dt_i}(\frac{|\vec{X}_n - \vec{x}_b|}{\alpha})\right) \\ &= \frac{i\omega_i q(t_i)}{4\pi|\vec{X}_n - \vec{x}_b|} \cdot \alpha^2(\vec{X}_n, \vec{x}_b, t_i)\beta(\vec{X}_n, \vec{x}_b, t_i),\end{aligned} \tag{22}$$

where

$$\begin{aligned}&\beta(\vec{X}_n, \vec{x}_b, t_i) \\ &= 1 + i\frac{\alpha}{\omega_i|\vec{X}_n - \vec{x}_b|}\frac{d}{dt_i}\left(\frac{|\vec{X}_n - \vec{x}_b|}{\alpha}\right) \\ &= 1 + i\frac{\alpha}{\omega_i}\left(\frac{c_0(1 - \alpha^{-1} + v^2/c_0^2)}{|\vec{X}_n - \vec{x}_b|} + \frac{\vec{x}_b - \vec{X}_n}{c_0 R_n}\cdot\frac{d\vec{v}}{dt_i}\right)\end{aligned} \tag{23}$$

α and $\vec{v}$ in these equations are $\alpha(\vec{X}_n, \vec{x}_b, t_i)$ and $\vec{v}(t_i)$. A more detailed derivation of Eq. (22) can be found in the monograph [36] (pp. 215–216). The frequency of the acoustic pressure $p(\vec{X}_n, \vec{x}_b, t_i)$ can be written as

$$\omega_i^n \triangleq \omega_i \cdot \alpha(\vec{X}_n, \vec{x}_b, t_i). \tag{24}$$

Consider the changing speed of α, β and R_n are much smaller than the angular frequency of the source, ω_i. Hence, in such a short duration the frequency of the rotating source is presumably frozen at ω_i^n. The corresponding result in the time-frequency domain by applying the continuous wavelet transform is

$$Y_n(\vec{X}_n, \vec{x}_b, \omega_i^n, t) = \frac{i\omega\alpha^2(\vec{X}_n, \vec{x}_b, t_i)\beta(\vec{X}_n, \vec{x}_b, t_i)}{4\pi|\vec{X}_n - \vec{x}_b|} q(t_i). \tag{25}$$

ACKNOWLEDGEMENTS

The authors thank Dr. Kenny Pok Wang Kwan for the proof-reading of this paper. X. Huang thanks Hong Kong University of Science and Technology for the support of his research collaboration.

REFERENCES

[1] B. D. Van Veen and K. M. Buckley, "Beamforming: A versatile approach to spatial filtering," *IEEE ASSP Mag.*, vol. 5, no. 2, pp. 4–24, Apr. 1988.
[2] J. Li and X. Zhang, "Direction of arrival estimation of quasi-stationary signals using unfolded coprime array," *IEEE Access*, vol. 5, pp. 6538–6545, 2017.
[3] H. Chen, H.-Z. Shao, and W.-Q. Wang, "Joint sparsity-based range-angle-dependent beampattern synthesis for frequency diverse array," *IEEE Access*, vol. 5, pp. 15152–15161, 2017.
[4] C. Mai, S. Lu, J. Sun, and G. Wang, "Beampattern optimization for frequency diverse array with sparse frequency waveforms," *IEEE Access*, vol. 5, pp. 17914–17926, 2017.
[5] R. O. Schmidt, "Multiple emitter location and signal parameter estimation," *IEEE Trans. Antennas Propag.*, vol. AP-34, no. 3, pp. 276–280, Mar. 1986.
[6] P. J. Chung and J. F. Böhme, "Comparative convergence analysis of EM and SAGE algorithms in DOA estimation," *IEEE Trans. Signal Process*, vol. 49, no. 12, pp. 2940–2949, Dec. 2001.
[7] R. Madan, N. B. Mehta, A. F. Molisch, and J. Zhang, "Energy-efficient decentralized cooperative routing in wireless networks," *IEEE Trans. Autom. Control*, vol. 54, no. 3, pp. 512–527, Mar. 2009.
[8] P. Stoica, Z. Wang, and J. Li, "Robust capon beamforming," *IEEE Signal Process. Lett.*, vol. 10, no. 6, pp. 172–175, Jun. 2003.
[9] J. Li and P. Stoica, *Robust Adaptive Beamforming*, vol. 88. Hoboken, NJ, USA: Wiley, 2005.
[10] R. A. Gramann and J. W. Mocio, "Aeroacoustic measurements in wind tunnels using adaptive beamforming methods," *J. Acoust. Soc. Amer.*, vol. 97, no. 6, pp. 3694–3701, 1995.
[11] X. Huang, L. Bai, I. Vinogradov, and E. Peers, "Adaptive beamforming for array signal processing in aeroacoustic measurements," *J. Acoust. Soc. Amer.*, vol. 131, no. 3, pp. 2152–2161, 2012.
[12] W. Zhou, Z. Ning, H. Li, and H. Hu, "An experimental investigation on rotor-to-rotor interactions of small UAV," in *Proc. 35th AIAA Appl. Aerodyn. Conf.* 2017, pp. 1–16.
[13] P. Sijtsma, "CLEAN based on spatial source coherence," *Int. J. Aeroacoust.*, vol. 6, no. 4, pp. 357–374, 1972.
[14] Y. Liu, A. R. Quayle, A. P. Dowling, and P. Sijtsma, "Beamforming correction for dipole measurement using two-dimensional microphone arrays," *J. Acoust. Soc. Amer.*, vol. 124, no. 1, pp. 182–191, 2008.

[15] X. Huang, X. Zhang, and Y. Li, "Broadband flow-induced sound control using plasma actuators," *J. Sound Vibrat.*, vol. 329, no. 13, pp. 2477–2489, 2010.
[16] X. Huang, "Real-time algorithm for acoustic imaging with a microphone array," *J. Acoust. Soc. Amer.*, vol. 125, no. 5, pp. EL190–EL195, 2009.
[17] X. Huang, "Real-time location of coherent sound sources by the observer-based array algorithm," *Meas. Sci. Technol.*, vol. 22, no. 4, pp. 065501-1–065501-9, 2011.
[18] X. Huang, "Compressive sensing and reconstruction in measurements with an aerospace application," *AIAA J.*, vol. 51, no. 4, pp. 1011–1015, 2013.
[19] S. Oerlemans, P. Sijtsma, and B. M. López, "Location and quantification of noise sources on a wind turbine," *J. Sound Vibrat.*, vol. 299, nos. 4–5, pp. 869–883, 2007.
[20] L. J. Heidelberg and D. G. Hall, "Inlet acoustic mode measurements using a continuously rotating rake," *J. Aircraft*, vol. 32, no. 4, pp. 761–767, 1995.
[21] D. Sutliff, "Turbofan duct mode measurements using a continuously rotating microphone rake," *Int. J. Aeroacoust.*, vol. 6, no. 2, pp. 147–170, 2007.
[22] R. P. Dougherty and B. E. Walker, "Virtual rotating microphone imaging of broadband fan noise," in *Proc. 30th AIAA Aeroacoust. Conf.*, 2009, pp. 1–14.
[23] P. Wolfram and M. Christian, "Rotating beamforming–motion-compensation in the frequency domain and application of high-resolution beamforming algorithms," *J. Sound Vibrat.*, vol. 333, no. 7, pp. 1899–1912, 2014.
[24] X. F. Zhang and D. Z. Xu, "Improved adaptive beamforming algorithm based on wavelet transform," in *Proc. Int. Conf. Commun., Circuits Syst.*, 2006, pp. 303–306.
[25] W. Xu, T.-C. Liu, and H. Schmidt, "Beamforming based on spatial-wavelet decomposition," in *Proc. Sensor Array Multichannel Signal Process. Workshop*, 2002, pp. 480–484.
[26] J. Wassermann, "Locating the sources of volcanic explosions and volcanic tremor at Stromboli Volcano (Italy) using beam-forming on diffraction hyperboloids," *Phys. Earth Planetary Interiors*, vol. 104, nos. 1–3, pp. 271–281, 1997.
[27] J. Xiang *et al.*, "Neuromagnetic correlates of developmental changes in endogenous high-frequency brain oscillations in children: A wavelet-based beamformer study," *Brain Res.*, vol. 1274, pp. 28–39, Jun. 2009.
[28] P. Sijtsma, "Using phased array beamforming to identify broadband noise sources in a turbofan engine," *Int. J. Aeroacoust.*, vol. 9, no. 3, pp. 357–374, 2010.
[29] P. Sijtsma, "CLEAN based on spatial source coherence," *Int. J. Aeroacoust.*, vol. 6, no. 4, pp. 357–374, 2007.
[30] S. Guérin and C. Weckmüller, "Frequency-domain reconstruction of the point-spread function for moving sources," in *Proc. BeBeC*, 2008, pp. 1–12.
[31] C. Michael, "Series expansion for the sound field of rotating sources," *J. Acoust. Soc. Amer.*, vol. 120, no. 3, pp. 1252–1256, 2006.
[32] M. Carley, "Inversion of spinning sound fields," *J. Acoust. Soc. Amer.*, vol. 125, no. 2, pp. 690–697, 2009.
[33] M. Carley, "Sound radiation from propellers in forward flight," *J. Sound Vibrat.*, vol. 225, no. 2, pp. 353–374, 1999.
[34] J. M. Lilly and S. C. Olhede, "Generalized morse wavelets as a superfamily of analytic wavelets," *IEEE Trans. Signal Process.*, vol. 60, no. 11, pp. 6036–6041, Nov. 2012.
[35] B. Chen, Q. Wei, T. Shao, Y. Li, and X. Huang, "Aeroacoustic imaging experiments of airframe noise in lined wall closed-section wind tunnel," *J. Aerosp. Eng.*, vol. 28, no. 4, pp. 04014090-1–04014090-8, 2014.
[36] S. W. Rienstra and A. Hirschberg, *An Introduction to Acoustics*. Eindhoven, The Netherlands: Eindhoven Univ. Technol., 2012.

WANGQIAO CHEN was born in Mudanjiang, China, in 1994. He received the B.Eng. degree from Peking University, Beijing, China, in 2016, where he is currently pursuing the Ph.D. degree in aerospace engineering. He was a Research Assistant with The Hong Kong University of Science and Technology from 2016 to 2017. His research interests include array signal processing, damage identification, and flow visualization for various aerospace applications. He was a recipient of the Silver Medal of the China's National Physics Olympiad in 2011.

XUN HUANG (M'17) was born in Hangzhou, China, in 1977. He received the B.Eng. degree in aerospace engineering from the Northwestern Polytechnical University, Xi'an, China, in 1999, the M.Eng. degree in automatic control from Tsinghua University, Beijing, China, in 2002, and the Ph.D. degree in aeronautics and astronautics from the University of Southampton, Southampton, U.K., in 2006. He was a Research Engineer with the Shanghai Control Laboratory, GE Global Research Center, in 2003, a Research Assistant in 2006, and became a Research Fellow in 2007. He was a Lecturer with the School of Engineering Sciences, University of Southampton, in 2008. From 2009 to 2016, he was an Associate Professor and, then, a Professor with the College of Engineering, Peking University. Since 2015, he has been visiting the University of Cambridge and The Hong Kong University of Science and Technology and initiating research collaboration. He has authored over 50 refereed journal papers and holds two patents. His research interests include control, acoustics, and array signal processing, especially for aerospace applications. He is an Editorial Board Member of the *Journal of Aeroacoustics* and the *Journal of Acta Mechanica Sinica*. He was a recipient of the Edison Technology Excellence Award in 2003, the Award of Excellent Young Scholar from the National Science Foundation of China in 2013, and the Newton Advanced Fellowship from the Royal Society, U.K., in 2015.